JCTC Journal of Chemical Theory and Computation

Article

pubs.acs.org/JCTC

Leveraging Symmetries of Static Atomic Multipole Electrostatics in Molecular Dynamics Simulations

Tristan Bereau,*[,†] Christian Kramer,*[,‡] and Markus Meuwly*[,†]

[†]Department of Chemistry, University of Basel, 4056 Basel, Switzerland

[‡]Institute of General, Inorganic and Theoretical Chemistry, and Center for Molecular Biosciences Innsbruck (CMBI), University of Innsbruck, 6020 Innsbruck, Austria

Supporting Information

ABSTRACT: Multipole (MTP) electrostatics provides the means to describe anisotropic interactions in a rigorous and systematic manner. A number of earlier molecular dynamics (MD) implementations have increasingly relied on the use of molecular symmetry to reduce the (possibly large) number of MTP interactions. Here, we present a CHARMM implementation of MTP electrostatics in terms of spherical harmonics. By relying on a systematic set of reference-axis systems tailored to various chemical environments, we obtain an implementation that is both efficient and scalable for (bio)molecular systems. We apply the method to a series of halogenated compounds to show (i) energy conservation; (ii) improvements in reproducing thermodynamic properties compared to standard point-charge (PC) models; (iii) performance of the code; and (iv) better stabilization of a brominated ligand in a target protein, compared to a PC force field. The implementation provides interesting perspectives toward a dual PC/MTP resolution, à la QM/MM.

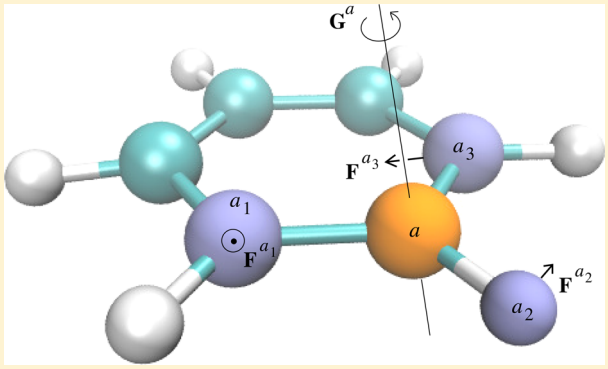

1. INTRODUCTION

Much of the prominence of electrostatics in chemical interactions arises from directionality: the relative stability of noncovalent geometries are often well described by the relative magnitude of their electrostatic energy.[1] In this regard, the evolution of atomistic force fields away from atomic point charges (PC) emanated from their limitations toward specific anisotropic features (e.g., lone pairs, hydrogen-bonding, π-electron density). The incorporation of off-site point charges—placed away from the nuclei—showed significant improvements in describing such anisotropic features.[1,2] While the method is both straightforward and computationally efficient, most of the applications available in the literature involve small molecules with few atoms. As a more systematic extension to PC force fields, multipole (MTP) electrostatics—a higher-order expansion of the electrostatic potential (ESP)—provides a rigorous framework to introduce anisotropic electrostatic features beyond the PC approximation (see, e.g., ref 3).

Stone, among others, pioneered the incorporation of MTPs in computational simulations of molecules by means of a spherical-harmonic expansion.[3−9] Early implementations represented the molecule's charge density through a set of MTPs associated with a single point (e.g., the molecule's center of mass). The expansion's convergence issues restricted the applicability of the method to small molecules—with limited success.[2] The natural extension of the method to MTPs centered on some (if not all) atomic sites proved more accurate. To determine the many parameters such an approach incumbs, Stone introduced the "Distributed Multipole Analysis" (DMA)—a fitting method that partitions the *ab initio* charge density into MTPs, in the spirit of a Mulliken population analysis (see ref 3 and references therein).

The most pressing issue that arises from the use of MTPs in molecular dynamics (MD) simulations is the shear number of interactions.[2,10] Leveraging symmetry to reduce the number of MTP coefficients can only speed up MD simulations if calculations are performed in the atoms' local frames. Working in the global frame, on the other hand, will require the multiplication of all MTPs to a rotation matrix. This process will, in general, transform any spherical tensor that carries a number of terms set to zero to a fully dimensional object (i.e., all components nonzero). Further, it will require the evaluation of all pair-interaction terms in the MTP calculation, preventing any computational speedup achieved on the basis of symmetry. We note, however, that such a global-frame approach benefits from simplified geometrical factors in the interaction potentials, thus standing as a potentially interesting methodology. To the best of our knowledge, a comparison of the computational performance of the two approaches has yet to be undertaken.

A number of MD implementations of MTP electrostatics have been reported. Leslie implemented the DMA method as an

Received: September 11, 2013
Published: November 5, 2013

extension to the DL_POLY package.[11] By defining spherical harmonics along the molecule's principle axes of inertia, one can take advantage of a number of symmetries for centrosymmetric molecules.[4,11,12] For instance, the aromatic carbon of a benzene cannot include any dipole moment along the normal to the ring.[10] Leslie's implementation was specifically tailored to organic crystals: Particle-Mesh Ewald is supported and the rigidity of molecules is enforced (i.e., no bond, angle, dihedral potentials). Still, efforts were made to reproduce the liquid properties of water and hydrogen fluoride.[13,14] Later, Plattner and Meuwly proposed a CHARMM implementation (available as the "MTP" module) of the DMA method, which includes fluctuating MTPs, for diatomic and triatomic molecules in the context of liquid and biomolecular simulations with particular emphasis on spectroscopic applications.[15,16] Their strategy followed Leslie's in aligning the local reference axis system along the molecule's principle axes of inertia. Clearly, such an approach is only suitable for small, rigid molecules: the mere presence of rotatable bonds will void most molecular symmetries. To go beyond small molecules, it is necessary to adjust the definition of the reference axis system to leverage local symmetries within the molecule. Such an effort was presented in the polarizable AMOEBA force field.[17] As atoms generate a variety of chemical environments, Kramer et al. recently developed a more systematic set of reference-axis systems that are oriented along major axes of symmetry.[18] We showed that their use could significantly cut down on the number of MTP coefficients—and thus interactions—in the context of condensed-phase simulations.[10]

In the present work, we propose a CHARMM implementation of MTP electrostatics (coined "MTPL" module) that is appropriate for arbitrarily large molecules. The use of the above-mentioned set of reference-axis systems that relate to the local chemical environment, rather than the entire molecule, provides both an efficient and systematic implementation for most (bio)molecular systems. We present our implementation in Section 2 and apply the method to a series of halogenated compounds in Section 3 to show that (i) our implementation conserves total energy; (ii) MTPs better reproduce thermodynamic properties of halobenzene compounds; (iii) the relative performance of MTP versus PC simulations becomes increasingly advantageous when MTPs are confined to a small part of the system (akin to a QM/MM treatment); and finally (iv) the interaction of a brominated ligand to a protein target is significantly stabilized from PC to MTP interactions, according to the relative free energy of binding.

2. IMPLEMENTATION

2.1. Force and Torque Calculation. We hereby describe our implementation of forces for the calculation of MTP interactions. We follow Stone and co-workers[3,6] for its notation and derivation of the forces and torques applied to MTPs up to quadrupoles. The directionality of nonmonopole coefficients requires the definition of a local axis system, for which we follow a systematic assignment[18] that exploits local symmetries. Since all coefficients are expressed in the atom's local frame, they are independent of orientation. The geometry of two atoms a and b relative to the orientation of their MTP sites is then computed by incorporating the unit vectors of their local axis systems $\{\mathbf{w}^a\} = \{\mathbf{x}^a,\mathbf{y}^a,\mathbf{z}^a\}$ and likewise for b. The set of $\{\mathbf{w}^a\}$ and $\{\mathbf{w}^b\}$ combined with the intersite unit vector $\hat{R}$ defines the direction cosines $\mathbf{q} = \{R,\mathbf{w}^a\cdot\hat{R},\mathbf{w}^b\cdot\hat{R},\mathbf{w}^a\cdot\mathbf{w}^b\}$ that provide a geometric description of the two MTP sites. From the interaction functions $T^{ab}_{tu}(\mathbf{q})$ for two MTP moments Q^a_t and Q^b_u of order t and u on atomic sites a and b, respectively, one can compute both the interaction energy

$$U^{ab}_{tu}(q) = Q_t{}^a Q_u{}^b T^{ab}_{tu}(q) \tag{1}$$

and the Kth component of the force F and torque G on site a:

$$F^a_K(q) = -Q_t{}^a Q_u{}^b \frac{\partial}{\partial A_K} T^{ab}_{tu}(q) \tag{2}$$

$$G^a_K(q) = -Q_t{}^a Q_u{}^b \frac{\partial}{\partial \theta^a_K} T^{ab}_{tu}(q) \tag{3}$$

where A_K and θ^a_K correspond to the translational and rotational (i.e., Euler angles[19] aligned with respect to $\{\mathbf{w}^a\}$) coordinates of the rigid body at site a, respectively. The force and torque acting on site b are expressed by differentiating $T^{ab}_{tu}(\mathbf{q})$ with respect to B_K and θ^b_K, respectively. Evidently, the interaction function contains the geometry-dependent information of the MTP interaction (e.g., $T^{ab}_{tu}(\mathbf{q}) = R^{-1}$ for the Coulomb interaction). While Stone describes the translation and rotation of the rigid body around its center of mass, we prescribe every site as the center of its own rigid body. We therefore avoid the summation found in the original force and torque definition, as well as simplify the torque expressions (Table 1), at the expense of a translational component exerted by the torque (see below). We point out the normalization difference between the direction-cosine terms $\mathbf{w}^a\cdot\hat{R}$, $\mathbf{w}^b\cdot\hat{R}$ that appear in the interaction functions and the terms present in Table 1: $\mathbf{w}^a\cdot\mathbf{R}$, $\mathbf{w}^b\cdot\mathbf{R}$. To relate one to the other, Stone derived the simple (but useful) relationship between the two expressions

Table 1. Table of Derivatives for the MTP Interactions Adapted from Stone[3] According to the Present Implementation (i.e., Every Atomic Site Is the Center of Its Own Rigid Body)[a]

	R	$\mathbf{w}^a\cdot\mathbf{R}$	$\mathbf{w}^b\cdot\mathbf{R}$	$\mathbf{w}^a\cdot\mathbf{w}^b$
$\partial/\partial A_K$	$-\hat{R}_K$	$-w^a_K$	$-w^b_K$	0
$\partial/\partial\theta^a_K$	0	$-(\mathbf{R}\times\mathbf{w}^a)_K$	0	$(\mathbf{w}^a\times\mathbf{w}^b)_K$
$\partial/\partial B_K$	$\hat{R}_K$	w^a_K	w^b_K	0
$\partial/\partial\theta^b_K$	0	0	$-(\mathbf{R}\times\mathbf{w}^b)_K$	$-(\mathbf{w}^a\times\mathbf{w}^b)_K$

[a]Such a prescription enforces several torque-related terms to zero.

$$\frac{\partial}{\partial C_K}(x^a\cdot\hat{R}) = \frac{1}{R}\left[\frac{\partial}{\partial C_K}(x^a\cdot\mathbf{R}) - (x^a\cdot\hat{R})\frac{\partial R}{\partial C_K}\right] \tag{4}$$

for the direction $\mathbf{x}^a$ and where C_K is one of the rigid-body coordinates (i.e., translation or rotation).

2.2. Example: The Dipole-Charge Interaction. All interaction functions have been published previously.[3,6] Because the derivation of forces and torques for all moments is straightforward but lengthy, we merely derive the simplest MTP interaction: dipole−charge. Its interaction function for the component α of a dipole moment $Q^a_{1\alpha}$ on site a and a charge Q^b_{00} on site b is written as $T^{ab}_{tu}(\mathbf{q}) = R^{-2}(\mathbf{w}^a_\alpha\cdot\hat{R})$. The force and torque expressions for atoms a and b (eq 2 and 3) are expressed from

$$\frac{\partial}{\partial C_K}T^{ab}_{tu}(\boldsymbol{q}) = -2R^{-3}(w^a_\alpha\cdot\hat{R})\frac{\partial R}{\partial C_K} + R^{-2}\frac{\partial}{\partial C_K}(w^a_\alpha\cdot\hat{R}) \tag{5}$$

where the last term expands to eq 4 and all derivatives are reported in Table 1. All other force and torque contributions can be found in Price et al.[6]

dx.doi.org/10.1021/ct400803f | J. Chem. Theory Comput. 2013, 9, 5450−5459

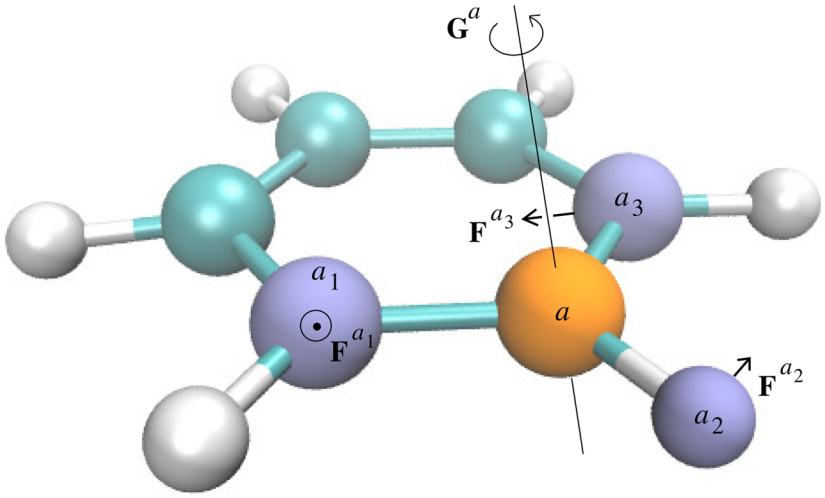

Figure 1. Cartoon representation of the torque propagation, $\mathbf{G}^a$, applied on MTP site a (colored in orange). The neighboring atoms a_1, a_2, and a_3 (colored in pastel blue) represent a's local axis system, which are used to propagate $\mathbf{G}^a$ via the—roughly sketched—forces $\mathbf{F}^{a1}$ (coming out of the page), $\mathbf{F}^{a2}$, and $\mathbf{F}^{a3}$. Though a torque oriented along one principal axis would generate forces lying in its orthogonal plane, the picture displays the more general case where the direction of $\mathbf{G}^a$ is arbitrary. For clarity, the translational force, $\mathbf{F}^a_{\text{trans}}$, is not shown. Rendered with VMD.[21]

2.3. Switching Functions for Finite-Cutoff Simulations. We adapted Stone's equations to include a polynomial-like switching function to smoothly taper each interaction function $T^{ab}_{tu}(\mathbf{q})$ to zero between the distances R_{on} and R_{off}

$$T^{ab}_{tu(\text{cut})}(\boldsymbol{q}, R_{\text{on}}, R_{\text{off}}) = T^{ab}_{tu}(\boldsymbol{q}) S(R, R_{\text{on}}, R_{\text{off}}) \tag{6}$$

where $R_{\text{on}} < R_{\text{off}}$, R_{off} corresponds to the cutoff distance, and $S(R,R_{\text{on}},R_{\text{off}})$ denotes the switching function

$$S(R, R_{\text{on}}, R_{\text{off}}) = \begin{cases} 1, & R < R_{\text{on}} \\ \dfrac{(R^2 - R^2_{\text{off}})^2 (R^2_{\text{off}} + 2R^2 - 3R^2_{\text{on}})}{(R^2_{\text{off}} - R^2_{\text{on}})^3}, & R_{\text{on}} < R < R_{\text{off}} \\ 0, & R > R_{\text{off}} \end{cases} \tag{7}$$

Its derivative is simply given by

$$S'(R, R_{\text{on}}, R_{\text{off}}) = \frac{\partial}{\partial R} S(R, R_{\text{on}}, R_{\text{off}}) = \begin{cases} \dfrac{12r(R^2 - R^2_{\text{off}})(R^2 - R^2_{\text{on}})}{(R^2_{\text{off}} - R^2_{\text{on}})^3}, & R_{\text{on}} < r < R_{\text{off}} \\ 0, & \text{otherwise} \end{cases} \tag{8}$$

Following the product rule for derivatives, switched forces and torques will contain two terms

$$F^a_{K(\text{cut})}(\boldsymbol{q}, R_{\text{on}}, R_{\text{off}}) = -Q_t{}^a Q_u{}^b \left[S(R, R_{\text{on}}, R_{\text{off}}) \frac{\partial}{\partial A_K} T^{ab}_{tu}(\boldsymbol{q}) + T^{ab}_{tu}(\boldsymbol{q}) \frac{\partial R}{\partial A_K} S'(R, R_{\text{on}}, R_{\text{off}}) \right] \tag{9}$$

$$G^a_{K(\text{cut})}(\boldsymbol{q}, R_{\text{on}}, R_{\text{off}}) = -Q_t{}^a Q_u{}^b S(R, R_{\text{on}}, R_{\text{off}}) \frac{\partial}{\partial \theta^a_K} T^{ab}_{tu}(\boldsymbol{q}) \tag{10}$$

The torque expression only contains one term because $\partial R/\partial \theta^a_K = 0$ in our implementation (see Table 1).

We note that several Particle-Mesh Ewald (PME) schemes for MTP interactions have been implemented.[11,20] While PME provides an elegant treatment of long-range electrostatics, we leave this for future work.

2.4. Torque Propagation. The torque G^a_K exerted on atom a must subsequently be propagated into forces. While the torque calculation applied on atom a considered it as a rigid body of its own (i.e., no other MTP site was involved), the propagation into forces will necessarily require other atoms to generate a rotation. We thus perform a rotation by exerting forces on the neighboring atoms involved in a's local reference axis system.[18] The torque is first projected along each principal axis of the rigid body's inertia tensor: $\{\mathbf{e}^a_1,\mathbf{e}^a_2,\mathbf{e}^a_3\}$, expressed in the atom's local axis system $\{\mathbf{w}^a\}$, with eigenvalues $\{\lambda^a_1,\lambda^a_2,\lambda^a_3\}$. The force applied on neighboring atom a_i, F^{ai}, is determined from the expression

$$F^{a_i} = \sum_{l=1}^{3} m_{a_i} \frac{(G^a \cdot \mathbf{e}^a_l)\mathbf{e}^a_l \times r}{\lambda^a_l} \tag{11}$$

where m_{ai} is the mass of atom a_i and $\mathbf{r}$ is the intersite vector between atom a and neighbor a_i (see Figure 1 for details). The translational component acting on a is simply given by the net force exerted by the collection of neighboring atoms: $\mathbf{F}^a_{\text{trans}} = -\sum_i \mathbf{F}^{ai}$.

2.5. Remarks. We point out a number of implementation details at this point:

- PC−PC interactions were *not* computed using the present implementation. Instead, we rely on existing implementations for Coulomb interactions (e.g., PME). We note that the above-mentioned use of switching functions would hardly be appropriate for PC−PC interactions, which decay as R^{-1}.
- To avoid spurious MTP moments that are close—but not equal—to zero, we only consider MTP moments that are larger than a certain threshold: $|Q_{kl}| \geq \varepsilon$. Here, $\varepsilon = 0.01$ in atomic units of the MTP moment is used.
- Because MTP interactions exert different power laws, we scale the cutoff distances accordingly. Table 2 details the switching-function parameters used in this work for each

Table 2. Switching-Function Parameters R_{on} and R_{off} for the Different Types of MTP Interactions (Up to Quadrupoles), Q_{lk}, Where l Denotes the Order of the Interaction and κ Runs over the Types of Interactions of That Order[a]

N	interactions	R_{on}	R_{off}
2	Q_{10}−Q_{00}	10	12
3	$Q_{2\kappa}$−Q_{00}, $Q_{1\kappa}$−$Q_{1\kappa}$	9	11
4	$Q_{2\kappa}$−$Q_{1\kappa}$	8	10
5	$Q_{2\kappa}$−$Q_{2\kappa}$	7	9

[a]The parameters are selected according to the power-law behavior of the interaction, R^{-N}. All distances are expressed in Å.

type of interaction. While the exponents of the power laws are comparatively small (i.e., $2 \le N \le 5$)—yielding longer-range interactions—most nonmonopole MTP moments are weak (see Section 3.2 and ref 10), such that we expect the bulk of MTP interactions to remain short-range. In addition, MTP interactions—unlike, for example, van der Waals interactions—can be both attractive and repulsive, thereby easily canceling each other in noncrystalline systems. These parameters can be changed by the user and have yet to be the subject of a detailed study.

- The implementation is fully parallelized and supports CHARMM's CRYSTAL image module.

3. APPLICATION: HALOGENATED COMPOUNDS

3.1. Simulation Methods. All simulations were performed in CHARMM using PME for the PC−PC interactions with grid-size spacing of 1 Å, relative tolerance of 10^{-6}, and interpolation order 4 for long-range electrostatics, and a 12 Å cutoff and 10 Å switching for the Lennard-Jones (LJ) interactions. All MTP interactions operated with power-law dependent switching functions, as described in Section 2.5. The MTPL module allows parallel simulations using the Message Passing Interface (MPI). *NPT* simulations were performed using the Hoover heat-bath method with pressure coupling[22] at T = 298 K, p = 1 atm, and the masses of the temperature and pressure piston to roughly 20% and 2% of the system's mass, respectively. Unless noted otherwise, the system was first minimized using steepest descent, then heated up at constant volume for 40 ps, followed by a 40-ps *NPT* equilibration using a Langevin damping coefficient on the piston γ_p = 20 ps^{-1}, and finally a 40-ps *NPT* production run. LJ long-range corrections were further applied to both the energy and the virial.[23]

3.1.1. Heat of Vaporization. A commonly used protocol[24−26] provides a convenient way to compute the heat of vaporization

$$\Delta H_{vap}(T) = E_{gas}(T) - E_{liq}(T) + RT \tag{12}$$

where E_{gas} and E_{liq} are the potential energies of one molecule in the gas and liquid (i.e., *NPT*) phases, respectively, and R is the gas constant. The gas-phase energy is computed from the minimized energy and the number of atoms, N, and constrained degrees of freedom, N_{cons}, in the molecule

$$E_{gas}(T) = E_{gas}^{minimized} + \frac{1}{2}RT(3N - 6 - N_{cons}) \tag{13}$$

3.1.2. Thermodynamic Integration. Free energies of hydration (i.e., solvation in water) and protein−ligand binding were computed using thermodynamic integration (TI). TI gradually couples/decouples chemical groups from the system by applying a parameter λ that scales the nonbonded interactions (i.e., LJ and PC/MTP electrostatics). The system's Hamiltonian is expressed as a function of λ to monitor the alchemical transformation

$$\Delta G_{A\to B} = \int_0^1 d\lambda \left\langle \frac{\partial H}{\partial \lambda} \right\rangle_\lambda \approx \sum_i (\lambda_{i+1} - \lambda_i) \left\langle \frac{\partial H}{\partial \lambda} \right\rangle_{\lambda_m} \tag{14}$$

where A→B refers to the alchemical transformation between compounds A and B, the canonical average $\langle\cdot\rangle_\lambda$ is performed over the phase space generated by H(λ), and $\lambda_m = (\lambda_i + \lambda_{i+1})/2$. LJ and PC derivatives were obtained from CHARMM 's PERT module, using soft-core potentials for the LJ interactions.[27,28] While we do not include LJ long-range corrections, we found no noticeable change when increasing the range of the interaction from a cutoff r_c = 12 Å (data not shown). The change in free energy due to MTP electrostatics with coupling λ_m was computed by first performing a simulation where we linearly scaled all MTP energies, forces, and torques by λ_m, for example,

$$U_{tu}^{ab}(q;\lambda_m) = \lambda_m Q_t^a Q_u^b T_{tu}^{ab}(q) \tag{15}$$

We then averaged over the solute−solute and solute−solvent energies (i.e., solvent−solvent interactions are not affected by λ_m) in such a way that its derivative with respect to λ yields the original energy. We first turned on the LJ interactions (with soft-core potentials), and later the electrostatics in the presence of the fully grown van der Waals radii, thereby avoiding the need for soft-core electrostatic potentials.

Using a thermodynamic cycle, the hydration free energy, ΔG_{hyd}, yields $\Delta G_{hyd} = \Delta G_{aqua} - \Delta G_{vac}$, where ΔG_{aqua} and ΔG_{vac} correspond to the free energy of insertion of the compound in a box of water and vacuum, respectively. For the water simulations, the solute was placed in a box of roughly 500 solvent molecules. We split each free-energy calculation in 20 evenly spaced λ windows between 0 and 1.

3.2. Force-Field Parametrization. In the following, we study a series of singly halogenated benzene (i.e., "PhX") compounds: PhH, PhF, PhBr, PhCl, and PhI, as well as pyrrole (used below in Section 3.6). PC and MTP parameters of each compound were derived from the ab initio (MP2 level with aug-cc-pVDZ basis set, except for iodine, where we used Wood-Boring effective core potentials[29]) electrostatic potential (ESP) of the gas-phase molecule, following refs 10 and 18. ESPs were fit to PC/MTP parameters in the first interaction belt (i.e., Lee-Richards molecular surfaces[30] of 1.66σ and 2.2σ, where σ is an atomic site's VDW radius). As for the Lennard-Jones parameters, we optimized both a series of ab initio gas-phase dimer energies and experimentally determined pure-liquid densities,[31] as described previously,[10] as well as heats of vaporization. Density and heat of vaporization are commonly used target quantities that constrain the sterics and strength of intermolecular interactions, respectively.[24,26] Tables S1 and S2 (Supporting Information) show the set of PC and MTP parameters used in this work, where the first column of the Table refers to the atom type, and the next four denote the atom's neighbors.[18] Figure 2 shows a comparison of the error in reproducing the ESP from (a) PC and (b) MTP (see caption for details). LJ coefficients parametrized against PC electrostatics are presented in Table 3, while a comparison between experimental data and simulations of the RMSE of gas-phase dimer energies, pure-liquid densities, heats of vaporization, and hydration free energies, are shown in Table 4. We note that our results for the halobenzene compounds are on par with the OPLS-AA forcefield,[32,33] in

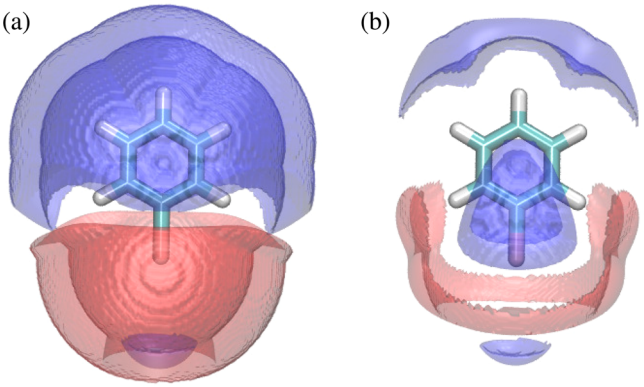

Figure 2. Isosurfaces of the difference between ab initio and (a) PC and (b) MTP ESPs of PhBr. Blue and red regions denote an error of +0.5 and −0.5 kcal/mol, respectively. The plots only show points within the first interaction belt.

Table 3. LJ Parameters ε and $R_{min}/2$ Parametrized Against PC and MTP Electrostatics[a]

		PC elec.		MTP elec.	
compound	atom name	ε	$R_{min}/2$	ε	$R_{min}/2$
PhH	C	−0.05	2.00	−0.08	2.00
	H	−0.05	1.30	−0.01	1.20
PhF	F	−0.15	1.10	−0.07	1.70
PhCl	Cl	−0.44	1.90	−0.29	2.00
PhBr	Br	−0.50	2.17	−0.46	2.30
PhI	I	−0.57	2.33	−0.53	2.43
pyrrole	N	−0.31	2.00	−0.11	2.20

[a]All units are in kcal/mol and Å.

terms of reproducing pure-liquid density, heat of vaporization, and hydration free energy. They underline that a careful PC parametrization can go a long way in reproducing the thermodynamic properties of many simple liquids (e.g., PhH, PhF), in which case MTPs are unlikely to play a significant role.

When switching from PC to MTP electrostatics, one should expect force-field reparametrization: standard parametrization protocols (including this one) make LJ coefficients inherently dependent on the force field's electrostatics. Lee and Meuwly recently reparametrized a MTP model of cyanide in water and showed that merely scaling the distance term, R_{min}, allowed to reproduce experimentally determined hydration free energies, vibrational relaxation times, and 1D/2D spectroscopies.[34−36] In the present work, however, we kept the protocol applied to PC electrostatics both for consistency and to best reproduce both sterics and energetics. The results are shown in Table 3. We find that most LJ coefficients remain similar across electrostatic representations, except for a comparatively large change for the well depth of N: 0.20 kcal/mol. The magnitude of these changes do not correlate with the impact on the hydration free energies: PhCl, PhBr, and PhI show the largest improvement in ΔG_{hyd}, though the changes in LJ parameters are modest. On the contrary, the large change of ε_N did not improve ΔG_{hyd}.

For all halobenzene compounds, MTP electrostatics allows us to reproduce hydration free energies within ≈0.15 kcal/mol of the experimental values. Naturally, we find the most significant improvements on PhCl, PhBr, and PhI, which carry strong σ holes. Jorgensen and Schyman introduced a correction for the OPLS-AA force field to better describe halogenated compounds by means of off-site point charges, which reproduces the hydration free energies of halobenzene compounds within 0.4 kcal/mol.[26] Other efforts to better reproduce σ holes in computer modeling include the work of Ibrahim on off-site point charges,[37] as well as careful electrostatic calculations from the SIBFA model[38] and a recently published polarizable ellipsoidal force field.[39]

Our PC and MTP parametrizations of pyrrole did not reproduce the experimental hydration free energy as well as for the other compounds, mostly due to the use of benzene's hydrogen atom type for pyrrole's amine. Clearly, the two types of hydrogens generate very different types of chemistry, which our PC and MTP force fields do distinguish (to the extent of the methods' resolutions). Using benzene's apolar hydrogen on the amine is a stretch of transferability that shows its limits. Likewise, distinguishing the carbons of benzene and pyrrole could prove more accurate, as pyrrole is more reactive. However, the sole purpose of the present pyrrole parametrization was to describe the amine group of the brominated ligand studied below (Section 3.6). Because the conclusions drawn in that application do not depend much on the quality of the amine's parametrization (we focus instead on the bromines), we decided against a careful, but more expensive, LJ parametrization of both atom types of that chemical group.

3.3. Structural Properties. We studied structural properties of the PhX compounds solvated in a box of 500 water molecules. *NPT* simulations were run for 1 ns, including 100 ps of equilibration. Figure 3 shows the radial distribution functions, $g(r)$, between the Br atom of PhBr with water oxygens for both PC and MTP electrostatics. The small changes in LJ parameters for Br led to virtually no difference in $g(r)$ between PC and MTP electrostatics, despite the large change in ΔG_{hyd} (Table 4). While

Table 4. Comparison between Experimental Results[25,31,40,41] and PC/MTP Calculations of Pure-Liquid Densities, ρ, Heats of Vaporization, ΔH_{vap}, and Hydration Free Energies, ΔG_{hyd}[a]

	exptl.			PC				MTP			
cmpd.	ρ	ΔH_{vap}	ΔG_{hyd}	RMSE	ρ	ΔH_{vap}	ΔG_{hyd}	RMSE	ρ	ΔH_{vap}	ΔG_{hyd}
PhH	0.88	7.89	−0.86	0.505	0.86	7.53	−0.77 ± 0.12	0.254	0.90	7.88	−0.89 ± 0.11
PhF	1.02	8.26	−0.80	1.215	1.05	7.95	−0.48 ± 0.30	0.502	1.05	8.60	−0.75 ± 0.08
PhCl	1.11	9.79	−1.12	0.929	1.11	9.68	−0.66 ± 0.01	0.464	1.14	10.13	−1.11 ± 0.26
PhBr	1.50	10.65	−1.46	1.173	1.44	10.54	−0.55 ± 0.04	0.682	1.47	11.98	−1.40 ± 0.10
PhI	1.83	11.85	−1.83	0.978	1.76	11.39	−1.35 ± 0.15	0.581	1.84	12.43	−1.97 ± 0.16
pyrrole	0.97	10.78	−4.78	1.212	1.00	11.11	−4.11 ± 0.04	1.092	0.99	10.87	−3.74 ± 0.20

[a]Root-mean squared errors (RMSEs) of gas-phase dimer energies (see ref 10) are also shown. All units are in kcal/mol, Å, and g/cm^3. The errors of the mean on the computed densities and heats of vaporization are 0.01 g/cm^3, and 0.05 kcal/mol, respectively, while they are mentioned explicitly for the hydration free energies.

dx.doi.org/10.1021/ct400803f | J. Chem. Theory Comput. 2013, 9, 5450−5459

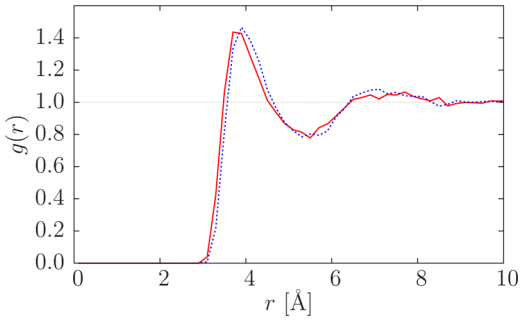

Figure 3. Radial distribution functions, $g(r)$, between the "Br" atom of PhBr with water oxygens for PC (red, solid line) and MTP (blue, dashed line) electrostatics.

no changes should be expected for large r given the range of MTP interactions, the change of electrostatic representation in the first peak (i.e., $r \approx 4$ Å) does not affect the radial distribution function in any significant way. We conclude that the influence of MTP electrostatics on PhBr's hydration free energy is too subtle and localized (i.e., MTP effects would primarily affect the first peak of $g(r)$, and such effects would likely be averaged over orientations) to be observed from the radial distribution function.

Likewise, PhCl and PhI, for which the MTP reparametrization involved small changes in the LJ parameters and significant improvements in ΔG_{hyd} (Table 4), showed no significant changes in $g(r)$ between electrostatic representations (data not shown).

3.4. Energy Conservation. A 12-water-molecule cluster provided a small-scale test for the conservation of total energy of our implementation. Due to the open boundary conditions, PME was replaced by real-space Coulomb electrostatics and an infinite cutoff was applied to all nonbonded interactions. Bonded and LJ parameters were obtained from the TIP3P parameters, while MTP coefficients are shown in Table 5—note that only the

Table 5. ESP-Fit MTPs ($l = 2$) for Water[a]

type	neighbors			MTP
H	O2	H	Q_{00}	+0.46
			Q_{00}	−0.92
O2	H	H	Q_{11s}	+0.18
			Q_{20}	−0.23

[a]Quality of the fit with respect to the ab initio ESP: root-mean squared error in the first interaction belt $\overline{\Delta E}$ = 0.43 kcal/mol for $l = 2$ (see ref 10 for details). Q_{lk} denotes the coefficient of the ESP's multipole expansion with l referring to the level of expansion of the ESP when performing the fit (e.g., $l = 0$ corresponds to PCs). The first column refers to the atom type and the next two denote the atom's neighbors (see ref 18 for more details on the atom-typing assignment). All units are in atomic units of the MTP moment.

oxygen carries higher MTP moments. A time step $\Delta t = 0.01$ fs was used for this system. Figure 4a shows the total energy as a function of time using harmonic bonded interactions. The fast oscillations—ultimately leading to a small energy drift—can be alleviated by constraining the bonded interactions, e.g., SHAKE[42] (Figure 4b). We argue that the fast oscillations present in the former case are largely due to the redistribution of oxygen torques solely on the lightweight hydrogens. A different implementation that computes the torque away from the oxygen may yield more stable dynamics in this rather special case. However, the common usage of bond-constraint algorithms for

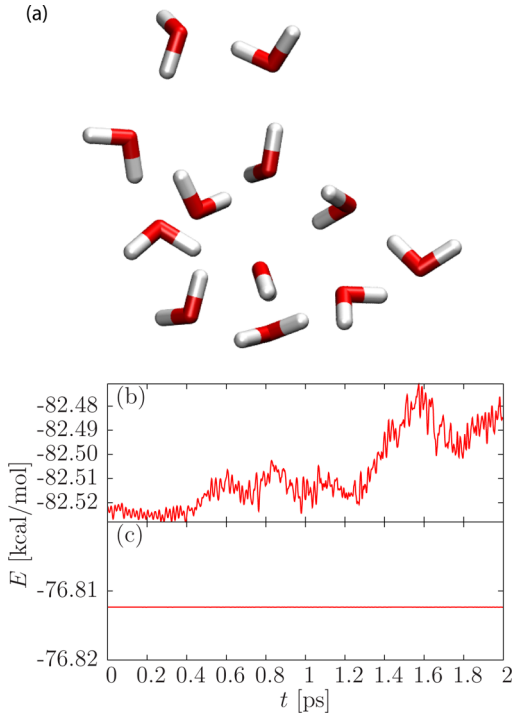

Figure 4. Total energy as a function of time for a simulation of 12 water molecules (see cartoon representation in part a) with open boundary conditions and MTP electrostatics using either (b) harmonic bonds or (c) SHAKE. In both cases, a time step $\Delta t = 0.01$ fs was used.

water makes this drawback of limited concern. The significant effect of SHAKE on energy conservation strongly suggests that the rapid oscillations seen in Figure 4a result from an incompatibility between the rigid-body approximation we invoked in the torque propagation (see Section 2.4) and the flexibility of bonded interactions in standard MD force fields. The collections of atoms used to convert torques into forces need to be strongly constrained to conserve energy. We thus encourage the use of bond-constraint algorithms, at least on hydrogens, when using the present MTP implementation. Most importantly, these results demonstrate the accuracy of the implementation of forces and torques.

Next, a larger system of 1000 water molecules provided a more realistic test scenario using a periodic box with PME electrostatics, bond constraints on all bonds to hydrogens using SHAKE, and long-range corrections for the LJ interactions. Prior to the *NVE* run, the simulation was equilibrated at atmospheric pressure and room temperature. We first minimized the system and ran the simulation with no initial velocities for 10 ps using the same time step $\Delta t = 0.01$ fs. The total energy exhibited no drift and oscillations of amplitude $\delta E \approx 0.08$ kcal/mol (data not shown), most likely resulting from a combination of fast dynamics, periodic boundary conditions, and PME-based PC-PC electrostatics. Interestingly, Leslie demonstrated energy conservation using PME-based MTP electrostatics and rigid-body dynamics, though the scale of his energy vs time plot does not allow to estimate the oscillation amplitudes.[11]

Finally, the energy conservation of pure-liquid benzene provided a similar size system, but with larger compounds. 150 molecules were initialized close to the system's average density at ambient temperature and pressure ($\rho_{exp} = 0.88$ g cm^{-3}), forming a cubic box of size 28 Å . Atomic MTPs were only assigned to the carbon atoms (see Supporting Information Table S1). We

dx.doi.org/10.1021/ct400803f | J. Chem. Theory Comput. 2013, 9, 5450−5459

performed several simulations with timesteps ranging from Δt = 0.005 to 0.1 fs for up to 100 ps. Figure 5 shows no systematic drift

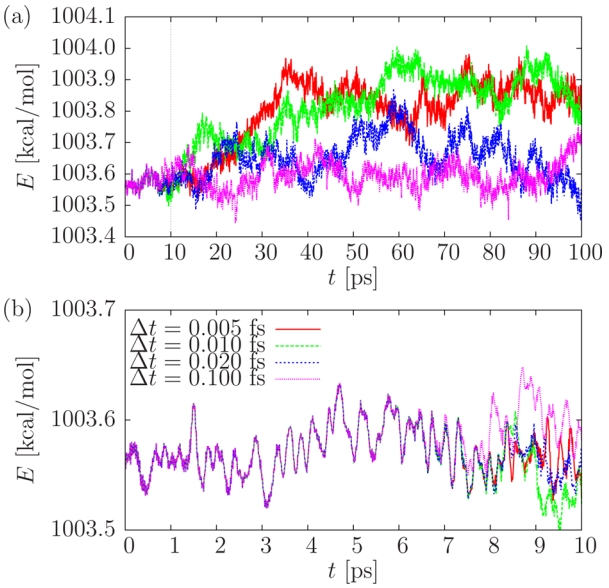

Figure 5. Total energy as a function of time for the pure-liquid benzene simulation with MTP electrostatics using various timesteps up to (a) 100 ps and (b) a close-up of the first 10 ps.

in the total energy and amplitudes $\delta E \approx 0.4$ kcal/mol. During the first 7 to 8 ps of the simulation (Figure 5b), all curves are virtually identical and oscillate within 0.1 kcal/mol. Following the above-mentioned water test case, we argue that these rapid oscillations are mainly due to torque propagations. While SHAKE had removed all oscillations from the small water-cluster simulation (Figure 4b), the same does not hold here. Oscillations are stronger than for the box of 1000 water molecules, suggesting the failure of our rigid-body approximation: though SHAKE effectively constrains the entire water molecule, benzene will still show significant intramolecular motion (e.g., C−C bond, angles, dihedrals). Unless one freezes *all* intramolecular interactions, energy oscillations will arise. Practically, we estimate from Figure 5b the rate of fast oscillations at around 0.05 kcal/mol per 0.5 ps, which translates into an instantaneous energy deviation of less than 10^{-7} kcal/mol per fs and per atom. This instantaneous drift has limited impact during the *NVE* simulations shown here and is altogether negligible in the presence of a thermostat. The present implementation is thus appropriate for *NVE* simulations—it does not require a thermostat to stabilize the system.

3.5. Performance. The added computational investment of MTP interactions, compared to PC, has always been a major reason why MTPs have not risen to mainstream use. The above-mentioned pure-liquid, periodic systems (i.e., water and benzene) provided benchmarks to compute the relative performance of MTP and PC simulations. The ratio of simulation times between MTP and PC electrostatics, $t^{\mathrm{MTP}}/t^{\mathrm{PC}}$, quantifies the added computational investment associated with MTPs. We propose to measure the relationship between simulation time and the number of intermolecular electrostatic pair interactions between two molecules, N_{int}. Three force fields are studied: "PC," "MTP without H," and "MTP with H," which denote the level of MTP expansion used and whether higher MTP parameters are present on H atoms ("MTP with H"). Note that the electrostatic parameters for water and benzene are shown in Table 5 and Supporting Information Table S1 for "MTP without H", while the "MTP with H" is not shown here. Since there are three atoms per water molecule, a dimer will contain $N_{\mathrm{int}}^{\mathrm{PC}} = 3 \times 3 = 9$ interactions for "PC," $N_{\mathrm{int}}^{\mathrm{MTP}} = 25$ interactions for "MTP without H" (see Table 5), and $N_{\mathrm{int}}^{\mathrm{MTP}} = 116$ for "MTP with H" (data not shown). Figure 6 shows the

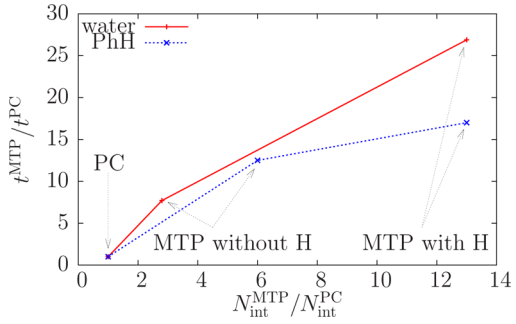

Figure 6. Relative performance between PC and MTP simulations. The plot shows the ratio of simulation time with MTP, t^{MTP}, and PC electrostatics, t^{PC} as a function of the ratio of the number of interactions between a homodimer with MTP, $N_{\mathrm{int}}^{\mathrm{MTP}}$, and PC electrostatics, $N_{\mathrm{int}}^{\mathrm{PC}}$. The two curves correspond to a box of 1000 water molecules (red, solid) and 150 PhH molecules (blue, dashed). "PC," "MTP without H," and "MTP with H" correspond to the number of PC/MTP parameters included in the fit and whether higher MTP parameters are included in H atoms ("MTP with H").

dependence of the ratios $t^{\mathrm{MTP}}/t^{\mathrm{PC}}$ with respect to $N_{\mathrm{int}}^{\mathrm{MTP}}/N_{\mathrm{int}}^{\mathrm{PC}}$. The two points that correspond to "PC" intercept the two axes at 1 by construction, the other ones relate the added time investment with the number of atom pairs in a dimer. The identical values obtained for the ratio $N_{\mathrm{int}}^{\mathrm{MTP}}/N_{\mathrm{int}}^{\mathrm{PC}}$ for "MTP with H" is purely coincidental. The computational slowdown, $t^{\mathrm{MTP}}/t^{\mathrm{PC}}$, ranges between 8−10 when MTPs are added to the heavy atoms only, and 15−25 when MTPs are included on all atoms. We find a strong correlation between the two quantities, suggesting that the performance of the code critically depends on the number of pair interactions involved. While the curve's behavior is roughly linear for water, the curve tends to saturate for the benzene system. The comparatively smaller computational investment of "MTP with H" in the case of benzene may be due to the larger size of benzene compared to water: the maximum intermolecular distance between two neighboring molecules is comparable to the interaction cutoff. We also find that the results depend very weakly on the range of the MTP interactions (see Section 2.5; data not shown). Overall, the results show that the added time investment of MTP interactions critically depends on the number of MTP pair interactions—highlighting the benefit of setting as many MTP coefficients as possible to zero.

When reducing the number of MTP parameters to a subset of the system, the computational performance is obviously improved: simulations of a single halobenzene compound solvated in roughly 500 molecules led to a computational slowdown $t^{\mathrm{MTP}}/t^{\mathrm{PC}} \approx 3.5$ between PC and MTP—a significant reduction compared to the pure-liquid benzene simulation (i.e., ≈13; see Figure 6). More significantly, applying MTP electrostatics on the ligand of a larger-scale (i.e., roughly 50 000 atoms) protein−ligand simulation (see Section 3.6 below) yielded a modest slowdown $t^{\mathrm{MTP}}/t^{\mathrm{PC}} \approx 1.2$. As the *ratio* of atoms carrying

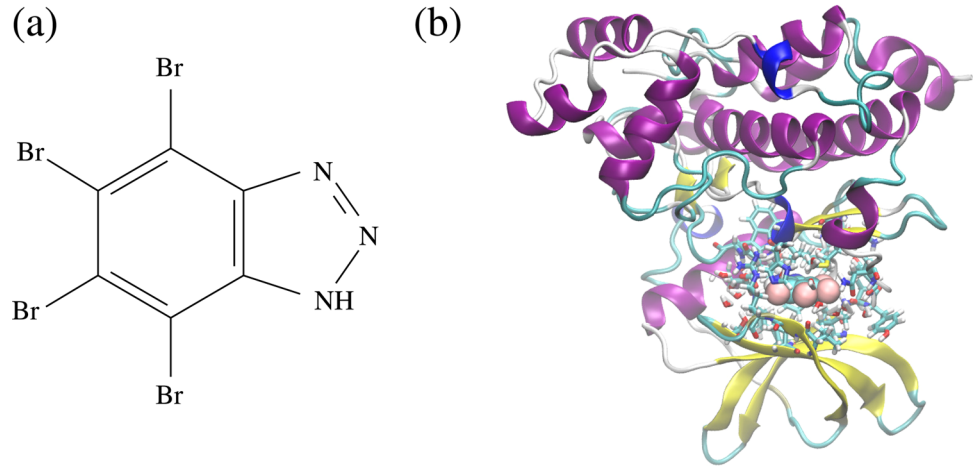

Figure 7. (a) Chemical structure of 4,5,6,7-tetrabromobenzotriazole and (b) cartoon representation of the protein−ligand complex: the secondary structure of the protein is shown in ribbons and coils, while the ligand is shown as bulky atoms and the neighboring protein pocket and water molecules are shown explicitly.

MTPs gets smaller, the computational performance tends toward the original PC protocol.

3.6. Protein−Ligand Binding. As a final application, protein−ligand binding provides a means to test the MTP implementation for large-scale, condensed-phase properties. Kolář and Hobza recently studied a series of brominated ligands binding to casein kinase 2 (CK2).[43] In the same spirit as Jorgensen's and Schyman's correction to the OPLS-AA force-field,[26] off-site point charges allowed a better description of the electrostatic potential of brominated ligands. By means of unconstrained MD simulations, they showed that a series of brominated ligands binding to CK2 were better stabilized using the additional point charges, though they did not compute free energies—only the root-mean squared distance of the ligand was computed. Here, we perform a comparative study of the binding of 4,5,6,7-tetrabromobenzotriazole with CK2 (PDB: 1J91;[44] experimentally determined free energy of binding is $\Delta G_{\mathrm{bind}}^{\mathrm{exp}} = -8.5$ kcal/mol[45]) using both PC and MTP electrostatics, see Figure 7. The above-mentioned force-field parametrization determined entirely the PC/MTP and LJ coefficients (Section 3.2), while the water, protein, and chloride-counterion parameters were those from the CHARMM22 force field.[46,47] We solvated and neutralized one monomer of CK2 from the crystal structure in a truncated octahedral box. Note that the reconstruction of hydrogens—absent from the crystal structure—led to an ambiguity as to the position of the triazole hydrogen: we positioned it toward CK2's ARG47, rather than PHE113, though it is unclear which conformation is favored. Restraining potentials on the ligand helped converge the sampling of the free-energy calculations, as described in refs 48−50. In the spirit of the above-mentioned hydration free-energy calculations (Section 3.2), TI was performed in both the protein and bulk water environments using the *NPT* ensemble. After a 120 ps equilibration simulation, used to estimate the parameters of the restraining potentials, we ran individual TI simulations with $\delta\lambda = 0.05$ spacings with a further 10-ps equilibration and 40-ps production runs. Running both forward and backward simulations allowed to check convergence and estimate error bars.

The protein−ligand free-energy difference between the ligand represented with PC and the same ligand represented with MTP electrostatics, $\Delta\Delta G_{\mathrm{bind}}^{\mathrm{PC}\rightarrow\mathrm{MTP}} = \Delta G_{\mathrm{bind}}^{\mathrm{MTP}} - \Delta G_{\mathrm{bind}}^{\mathrm{PC}}$, quantifies the relative stability of PC and MTP simulations. We obtain a free-energy difference $\Delta\Delta G_{\mathrm{bind}}^{\mathrm{PC}\rightarrow\mathrm{MTP}} = -3.8 \pm 0.3$ kcal/mol, meaning that MTP electrostatics indeed provides improved stability to the compound. Interestingly, this figure closely matches the added hydration free energy provided by all four bromine atoms (Table 4), though the partial burying of the ligand in the pocket surely thwarts such a simple analysis. The results are on par with the conclusions of Kolář and Hobza, who observed increased stability with off-site PCs, compared to a standard PC force field.

4. CONCLUSIONS

We propose an implementation of nonpolarizable, static atomic MTP electrostatics for atomistic MD simulations. Addressing computational concerns, we reduce the large number of MTP interactions (up to quadrupoles in this work) by using a systematic set of reference axis systems that exploit symmetries. These axis systems can thus reduce the number of interaction terms by setting certain coefficients to zero,[10,18] while the computation of interaction energies, forces, and torques is performed in the atoms' local reference frames to avoid contaminating null coefficients from other components.

We demonstrated the energy-conservation capabilities of the MTP implementation: strict conservation is ensured for small water clusters, while larger, periodic systems suffer from fast dynamics. We obtain better stability when using bond-constraint algorithms (e.g., SHAKE), which help satisfy the rigid-body approximation assumed in the propagation of the torques into forces on neighboring atoms.

The comparative parametrization of halobenzene compounds illustrated how nonpolarizable MTP electrostatics can overcome certain limitations of standard PC force fields. In this case, MTP interactions provide a significantly better description of the σ hole present in the stronger halogens. The MTP parametrization presented here reproduces both ab initio calculations and thermodynamic properties (i.e., pure-liquid density, heat of vaporization, and hydration free energy) with excellent agreement compared to experiment. Due to the intrinsic dependence of LJ parameters on the electrostatics, we have found it necessary to reparametrize all LJ coefficients between PC and MTP force fields. Overall, the results show that MTP force fields are not necessary to reproduce the thermodynamic properties of simple compounds (e.g., PhH, PhF). They do provide significant

improvements in cases where anisotropic electrostatic features are significant (e.g., PhCl, PhBr, PhI). It remains to be seen how the use of MTP force fields can improve dynamical properties. Clearly, the limits of the PC and MTP representations can only be probed against accurate force fields—a somewhat evident conclusion that bears significance when choosing between the two: a tailor-made PC force field may well perform better than a generic MTP force field.

Finally, we presented protein−ligand binding calculations of a brominated ligand to casein kinase 2. Comparative free-energy calculations of the PC and MTP force fields show significant improvement in binding when using MTPs on the ligand and require negligible additional computational investment.

The computational performance of the MTP module becomes quite advantageous when limiting MTPs to a small collection of atoms in the simulation. In the spirit of QM/MM methodologies (see, e.g., ref 51) and recently developed adaptive resolution schemes,[52] which both couple different representations within a simulation, applying MTP electrostatics to a subsystem provides a locally enhanced description. Cross-interactions across the two electrostatic representations is provided by simple PC-MTP products and the Lorentz−Berthelot mixing rule for electrostatic and LJ interactions, respectively. Additionally, the parametrization scheme used in this work constrained the MTP monopoles around values obtained from a standard PC fit, thereby producing reasonable PC−PC interactions at the interface between the MTP and PC atoms. Whether and in what range such cross-interaction is accurate enough has yet to be investigated. As it stands, locally enhancing the system using MTP electrostatics can provide a promising alternative to more expensive methods, such as QM/MM,[51] the Car−Parrinello method,[53] or polarizable force fields (e.g., SIBFA,[54−57] AMOEBA,[17] and others that are specific to a few molecules[58,59]), in case polarization is not a critical issue.

■ ASSOCIATED CONTENT

Supporting Information

Electrostatic parameters (both PC and MTP) for the halogenated compounds, pyrrole, hexabromobenzene, and 4,5,6,7-tetrabromobenzotriazole. This material is available free of charge via the Internet at http://pubs.acs.org.

■ AUTHOR INFORMATION

Corresponding Authors

*E-mail: bereau@alumni.cmu.edu.
*E-mail: christian.kramer@uibk.ac.at.
*E-mail: m.meuwly@unibas.ch.

Notes

The authors declare no competing financial interest.

■ ACKNOWLEDGMENTS

We acknowledge financial support from the Swiss National Science Foundation (Grant 200020-132406 and the NCCR MUST).

■ REFERENCES

(1) Kollman, P. A. Noncovalent interactions. *Acc. Chem. Res.* **1977**, *10*, 365−371.
(2) Brobjer, J. T.; Murrell, J. N. A method for calculating the electrostatic energy between small polar molecules. The multipole-fitted point-charge method. *J. Chem. Soc. Far. Trans.* **1982**, *78*, 1853−1870.
(3) Stone, A. J. *The Theory of Intermolecular Forces*; Clarendon Press: Oxford, 1996; Vol. 32.
(4) Gray, C. Spherical tensor approach to multipole expansions. I. Electrostatic interactions. *Can. J. Phys.* **1976**, *54*, 505−512.
(5) Stone, A. The description of bimolecular potentials, forces and torques: the S and V function expansions. *Mol. Phys.* **1978**, *36*, 241−256.
(6) Price, S.; Stone, A.; Alderton, M. Explicit formulae for the electrostatic energy, forces, and torques between a pair of molecules of arbitrary symmetry. *Mol. Phys.* **1984**, *52*, 987−1001.
(7) Vigné-Maeder, F.; Claverie, P. The exact multicenter multipolar part of a molecular charge distribution and its simplified representations. *J. Chem. Phys.* **1988**, *88*, 4934.
(8) Hättig, C. Recurrence relations for the direct calculation of spherical multipole interaction tensors and Coulomb-type interaction energies. *Chem. Phys. Lett.* **1996**, *260*, 341−351.
(9) Hättig, C. On the calculation of derivatives for Coulomb-type interaction energies and general anisotropic pair potentials. *Chem. Phys. Lett.* **1997**, *268*, 521−530.
(10) Bereau, T.; Kramer, C.; Monnard, F. W.; Nogueira, E. S.; Ward, T. R.; Meuwly, M. Scoring multipole electrostatics in condensed-phase atomistic simulations. *J. Phys. Chem. B* **2013**, *117*, 5460−5471.
(11) Leslie, M. DL_MULTI−A molecular dynamics program to use distributed multipole electrostatic models to simulate the dynamics of organic crystals. *Mol. Phys.* **2008**, *106*, 1567−1578.
(12) Buckingham, A.; Fowler, P.; Hutson, J. M. Theoretical studies of van der Waals molecules and intermolecular forces. *Chem. Rev.* **1988**, *88*, 963−988.
(13) Liem, S.; Popelier, P.; Leslie, M. Simulation of liquid water using a high-rank quantum topological electrostatic potential. *Int. J. Quantum Chem.* **2004**, *99*, 685−694.
(14) Liem, S.; Popelier, P. High-rank quantum topological electrostatic potential: Molecular dynamics simulation of liquid hydrogen fluoride. *J. Chem. Phys.* **2003**, *119*, 4560.
(15) Plattner, N.; Meuwly, M. The role of higher CO-multipole moments in understanding the dynamics of photodissociated carbon-monoxide in myoglobin. *Biophys. J.* **2008**, *94*, 2505−2515.
(16) Plattner, N.; Meuwly, M. Higher order multipole moments for molecular dynamics simulations. *J. Mol. Model.* **2009**, *15*, 687−694.
(17) Ponder, J. W.; Wu, C.; Ren, P.; Pande, V. S.; Chodera, J. D.; Schnieders, M. J.; Haque, I.; Mobley, D. L.; Lambrecht, D. S.; DiStasio, R. A., Jr; Head-Gordon, M.; Clark, G. N. I.; Johnson, M. E.; Head-Gordon, T. Current status of the AMOEBA polarizable force field. *J. Phys. Chem. B* **2010**, *114*, 2549−2564.
(18) Kramer, C.; Gedeck, P.; Meuwly, M. Atomic multipoles: Electrostatic potential fit, local reference axis systems, and conformational dependence. *J. Comput. Chem.* **2012**, *33*, 1673−1688.
(19) Goldstein, H.; Poole Jr., C. P.; Safko, J. L. *Classical Mechanics*, 3rd ed.; Addison-Wesley: Boston, 2001.
(20) Sagui, C.; Pedersen, L. G.; Darden, T. A. Towards an accurate representation of electrostatics in classical force fields: Efficient implementation of multipolar interactions in biomolecular simulations. *J. Chem. Phys.* **2004**, *120*, 73.
(21) Humphrey, W.; Dalke, A.; Schulten, K. VMD: Visual molecular dynamics. *J. Mol. Graphics* **1996**, *14*, 33−38.
(22) Feller, S. E.; Zhang, Y.; Pastor, R. W.; Brooks, B. R. Constant pressure molecular dynamics simulation: The Langevin piston method. *J. Chem. Phys.* **1995**, *103*, 4613.
(23) Allen, M. P.; Tildesley, D. J. *Computer Simulation of Liquids*; Oxford University Press: New York, 1989.
(24) Vanommeslaeghe, K.; Hatcher, E.; Acharya, C.; Kundu, S.; Zhong, S.; Shim, J.; Darian, E.; Guvench, O.; Lopes, P.; Vorobyov, I.; Mackerell, A. D. CHARMM general force field: A force field for drug-like molecules compatible with the CHARMM all-atom additive biological force fields. *J. Comput. Chem.* **2010**, *31*, 671−690.
(25) Wang, J.; Hou, T. Application of molecular dynamics simulations in molecular property prediction. 1. Density and heat of vaporization. *J. Chem. Theory Comp.* **2011**, *7*, 2151−2165.
(26) Jorgensen, W. L.; Schyman, P. Treatment of halogen bonding in the OPLS-AA force field: Application to potent anti-HIV agents. *J. Chem. Theory Comp.* **2012**, *8*, 3895−3901.

(27) Zacharias, M.; Straatsma, T.; McCammon, J. Separation-shifted scaling, a new scaling method for Lennard-Jones interactions in thermodynamic integration. *J. Chem. Phys.* **1994**, *100*, 9025−9031.
(28) Boresch, S. The role of bonded energy terms in free energy simulations—Insights from analytical results. *Mol. Sim.* **2002**, *28*, 13−37.
(29) Wood, J. H.; Boring, A. M. Improved Pauli Hamiltonian for local-potential problems. *Phys. Rev. B* **1978**, *18*, 2701−2711.
(30) Lee, B.; Richards, F. M. The interpretation of protein structures: Estimation of static accessibility. *J. Mol. Biol.* **1971**, *55*, 379−400.
(31) Lide, D. R. *CRC Handbook of Chemistry and Physics*; CRC press: Boca Raton, FL, 2012.
(32) Jorgensen, W. L.; Maxwell, D. S.; Tirado-Rives, J. Development and testing of the OPLS all-atom force field on conformational energetics and properties of organic liquids. *J. Am. Chem. Soc.* **1996**, *118*, 11225−11236.
(33) Jorgensen, W. L.; Ulmschneider, J. P.; Tirado-Rives, J. Free energies of hydration from a generalized born model and an all-atom force field. *J. Phys. Chem. B.* **2004**, *108*, 16264−16270.
(34) Lee, M. W.; Meuwly, M. *Phys. Chem. Chem. Phys.* **2013**, DOI: 10.1039/c3cp52713a.
(35) Lee, M. W.; Meuwly, M. On the role of nonbonded interactions in vibrational energy relaxation of cyanide in water. *J. Phys. Chem. A* **2011**, *115*, 5053−5061.
(36) Lee, M. W.; Carr, J. K.; Göllner, M.; Hamm, P.; Meuwly, M. 2D IR spectra of cyanide in water investigated by molecular dynamics simulations. *J. Chem. Phys.* **2013**, *139*, 054506.
(37) Ibrahim, M. A. Molecular mechanical study of halogen bonding in drug discovery. *J. Comput. Chem.* **2011**, *32*, 2564−2574.
(38) Hage, K. E.; Piquemal, J.-P.; Hobaika, Z.; Maroun, R. G.; Gresh, N. Could an anisotropic molecular mechanics/dynamics potential account for sigma hole effects in the complexes of halogenated compounds? *J. Comput. Chem.* **2013**, 1125.
(39) Du, L.; Gao, J.; Bi, F.; Wang, L.; Liu, C. A polarizable ellipsoidal force field for halogen bonds. *J. Comput. Chem.* **2013**, 2032.
(40) Riddick, J. A.; Bunger, W. B.; Sakano, T. K. *Organic Solvents: Physical Properties and Methods of Purification*; John Wiley and Sons: New York, 1986.
(41) Gerber, P. R. Charge distribution from a simple molecular orbital type calculation and non-bonding interaction terms in the force field MAB. *J. Comput.-Aided Mol. Des.* **1998**, *12*, 37−51.
(42) Ryckaert, J.-P.; Ciccotti, G.; Berendsen, H. J. Numerical integration of the cartesian equations of motion of a system with constraints: molecular dynamics of *n*-alkanes. *J. Comput. Phys.* **1977**, *23*, 327−341.
(43) Kolář, M.; Hobza, P. On extension of the current biomolecular empirical force field for the description of halogen bonds. *J. Chem. Theory Comp.* **2012**, *8*, 1325−1333.
(44) Battistutta, R.; De Moliner, E.; Sarno, S.; Zanotti, G.; Pinna, L. A. Structural features underlying selective inhibition of protein kinase CK2 by ATP site-directed tetrabromo-2-benzotriazole. *Protein Sci.* **2001**, *10*, 2200−2206.
(45) Bortolato, A.; Moro, S. In silico binding free energy predictability by using the linear interaction energy (LIE) method: Bromobenzimidazole CK2 inhibitors as a case study. *J. Chem. Inf. Model.* **2007**, *47*, 572−582.
(46) MacKerell, A. D.; Bashford, D.; Bellott, M.; Dunbrack, R.; Evanseck, J.; Field, M. J.; Fischer, S.; Gao, J.; Guo, H.; Ha, S.; Joseph-McCarthy, D.; Kuchnir, L.; Kuczera, K.; Lau, F. T. K.; Mattos, C.; Michnick, S.; Ngo, T.; Nguyen, D. T.; Prodhom, B.; Reiher, W. E.; Roux, B.; Schlenkrich, M.; Smith, J. C.; Stote, R.; Straub, J.; Watanabe, M.; Wiórkiewicz- Kuczera, J.; Yin, D.; Karplus, M. All-atom empirical potential for molecular modeling and dynamics studies of proteins. *J. Phys. Chem. B* **1998**, *102*, 3586−3616.
(47) MacKerell, A. D.; Feig, M.; Brooks, C. L. Extending the treatment of backbone energetics in protein force fields: Limitations of gas-phase quantum mechanics in reproducing protein conformational distributions in molecular dynamics simulations. *J. Comput. Chem.* **2004**, *25*, 1400−1415.
(48) Boresch, S.; Tettinger, F.; Leitgeb, M.; Karplus, M. Absolute binding free energies: A quantitative approach for their calculation. *J. Phys. Chem. B* **2003**, *107*, 9535−9551.
(49) Mobley, D. L.; Chodera, J. D.; Dill, K. A. On the use of orientational restraints and symmetry corrections in alchemical free energy calculations. *J. Chem. Phys.* **2006**, *125*, 084902.
(50) Deng, Y.; Roux, B. Computations of standard binding free energies with molecular dynamics simulations. *J. Phys. Chem. B* **2009**, *113*, 2234−2246.
(51) Lin, H.; Truhlar, D. G. QM/MM: What have we learned, where are we, and where do we go from here? *Theor. Chem. Acc.* **2007**, *117*, 185−199.
(52) Potestio, R.; Fritsch, S.; Espanol, P.; Delgado-Buscalioni, R.; Kremer, K.; Everaers, R.; Donadio, D. Hamiltonian adaptive resolution simulation for molecular liquids. *Phys. Rev. Lett.* **2013**, *110*, 108301.
(53) Car, R.; Parrinello, M. Unified approach for molecular dynamics and density-functional theory. *Phys. Rev. Lett.* **1985**, *55*, 2471.
(54) Gresh, N.; Claverie, P.; Pullman, A. Intermolecular interactions: Reproduction of the results of ab initio supermolecule computations by an additive procedure. *Int. J. Quantum Chem.* **1979**, *16*, 243−253.
(55) Gresh, N.; Claverie, P.; Pullman, A. Theoretical studies of molecular conformation. Derivation of an additive procedure for the computation of intramolecular interaction energies. Comparison with ab initio SCF computations. *Theor. Chim. Acta* **1984**, *66*, 1−20.
(56) Gresh, N.; Pullman, A.; Claverie, P. Theoretical studies of molecular conformation. II: Application of the SIBFA procedure to molecules containing carbonyl and carboxylate oxygens and amide nitrogens. *Theor. Chim. Acta* **1985**, *67*, 11−32.
(57) Gresh, N.; Claverie, P.; Pullman, A. Intermolecular interactions: Elaboration on an additive procedure including an explicit charge-transfer contribution. *Int. J. Quantum Chem.* **1986**, *29*, 101−118.
(58) Ren, P.; Ponder, J. W. Polarizable atomic multipole water model for molecular mechanics simulation. *J. Phys. Chem. B* **2003**, *107*, 5933−5947.
(59) Jiao, D.; King, C.; Grossfield, A.; Darden, T. A.; Ren, P. Simulation of Ca^{2+} and Mg^{2+} solvation using polarizable atomic multipole potential. *J. Phys. Chem. B* **2006**, *110*, 18553−18559.